

# EXTENSIVE SPIRAL STRUCTURE AND COROTATION RESONANCE

Blaise Canzian<sup>1</sup>

*Universities Space Research Association,  
U.S. Naval Observatory, and  
Space Telescope Science Institute(email: blaise@nofs.navy.mil)*

## ABSTRACT

Spiral density wave theories demand that grand design spiral structure be bounded, at most, between the inner and outer Lindblad resonances of the spiral pattern. The corotation resonance lies between the outer and inner Lindblad resonances. The locations of the resonances are at radii whose ratios to each other are rather independent of the shape of the rotation curve. The measured ratio of outer to inner extent of spiral structure for a given spiral galaxy can be compared to the standard ratio of corotation to inner Lindblad resonance radius. In the case that the measured ratio far exceeds the standard ratio, it is likely that the corotation resonance is within the bright optical disk. Studying such galaxies can teach us how the action of resonances sculpts the appearance of spiral disks. This paper reports observations of 140 disk galaxies, leading to resonance ratio tests for 109 qualified spirals. It lists candidates that have a good chance of having the corotation resonance radius within the bright optical disk.

*Subject headings:* galaxies: kinematics and dynamics; galaxies: spiral; galaxies: structure

---

<sup>1</sup>Postal address: U.S. Naval Observatory, PO Box 1149, Flagstaff, AZ 86002

## 1. Introduction

Disk galaxies exhibit many designs: bars, rings, and spiral structure. The structure and placement of rings and bars are widely believed, on numerical and analytical grounds, to be governed by resonance. A resonance is a rational relationship between two frequencies. Inner and outer rings form at radii that are resonant with the angular frequency of the bar pattern (Schwarz 1981; Buta 1986; Buta & Crocker 1991). A strong bar ends near its corotation resonance (Contopoulos 1980), referred to hereafter as “CR”.

Many disk galaxies show spiral patterns, some of which are beautiful, two-armed spirals. What effect do resonances have on the appearance of spiral patterns? First consider barred spirals. It was once widely believed that the bar was capable of “driving” spiral structure (e.g., van Albada & Roberts 1981) or of providing a source of disturbances that might be swing amplified into spiral structure (Toomre 1977). Then the bar and the spiral patterns would be resonantly related. But Sellwood & Sparke (1988) have suggested that spiral patterns need not be resonantly related to bars. Kinematic data for few galaxies have been analyzed to see if the resonant link exists between bars and spirals. Bar and spiral are part of the same pattern in both NGC1365 and NGC4321, for example, but the transition from bar to spiral is at the CR in NGC1365 (Lindblad, Lindblad, & Athanassoula 1996) while it is at the inner 4:1 resonance in NGC4321 (Elmegreen, Elmegreen, & Montenegro 1992; Sempere et al. 1995; Canzian & Allen 1997). Apart from these two galaxies, there are differences between strongly and weakly barred spirals to consider, as well as differences between flat and exponential bars.

Spiral patterns exist in disks without bars, too. Spiral density waves are constrained to exist between the inner and outer Lindblad resonances, hereafter “ILR” and “OLR”. Aside from this constraint, the role of resonances in shaping

pure spiral morphology is uncertain.

Many signatures of resonance structures have been suggested and used with varying success. Dust lanes may jump to the other sides of spiral arms across the CR (Roberts 1969). Star formation may be less efficient within spiral arms near CR (seen in NGC0628 and NGC3992 by Cepa & Beckman 1990 and in M51 by Knapen et al. 1992 but not in NGC4321 by Knapen et al. 1996). Enhanced star formation may occur in the interarm region at the CR, and at the inner 4:1 resonance there may be brightness minima in the arms and spurs should erupt in the interarm region (Elmegreen et al. 1989, 1992). Not all of the above prescriptions work in all cases.

Tests of the above prescriptions can follow only when clear determinations of resonance locations have been made for many spirals. Confirmation of resonance locations requires kinematic data. Such data derive from emission line mapping, which is difficult and time consuming. It would be more rewarding to study galaxies for which interesting resonance locations were known beforehand to be at easily studied radii in the bright disk. The CR is one of the most interesting resonances to study.

This paper presents a test to identify galaxies whose CR is favorably placed for study (within the bright disk). The test requires only moderately deep imaging in typical seeing. No rotation curve data are necessary. The test is not completely determinate: galaxies with CR within the bright disk can be missed. This is the price paid for operating in ignorance of the rotation curve shape and spiral pattern speed. However, the test is reliable: when a suitable galaxy is identified, there is a good chance that its CR is, indeed, within the bright disk.

The basis of the test to identify galaxies with well-placed CR is presented in §2. The section also investigates how much effect the shape of the rotation curve and the spiral pattern speed have on the outcome of the test. §3 outlines the observations. The analysis of the imaging is described

in §4. This includes not only a description of the measurements made but also some surface photometry to estimate how deep the imaging reaches. The results are presented in §5, where promising galaxies are described and where the different characteristics of barred and pure spirals are discussed.

## 2. Extensive spiral structure

Spiral structure is constrained to be between the ILR and OLR of the spiral pattern. The CR is between the ILR and OLR. It is not known how often spiral structure remains relatively bright, or even optically detectable, at radii approaching the OLR. Spiral structure is probably detectable at the CR in most galaxies. We seek galaxies for which the spiral structure is not merely detectable, but is genuinely bright, at the CR. By implication, the spiral structure would then stretch most of the way between the ILR and OLR.

To test for placement of the CR within the bright disk, first measure the inner and outer extent of the spiral structure from deep imaging in typical seeing. When the measured ratio of the outer to inner extent exceeds the “typical” ratio of CR to ILR radius (described in §2.1), the spiral structure appears to have needed more space than is available just between the ILR and CR. Therefore, the CR is in the optically detectable part of the disk. The larger the measured ratio, the deeper into the bright part of the disk the CR might be.

### 2.1. Flat rotation curve

Consider a flat rotation curve. (More realistic shapes will be considered in §2.2.) At the CR, disk material has an orbital frequency equal to the angular frequency of the spiral pattern: the stars and pattern corotate. That is,

$$\Omega_p = V/R_{\text{CR}} \quad (1)$$

at the CR, where  $\Omega_p$  is the pattern angular frequency,  $V$  is the circular rotation speed, and  $R_{\text{CR}}$

is the corotation resonance radius. At the Lindblad resonances, the material experiences the entire pattern exactly once each orbit. At the ILR, the material sweeps through the pattern, while at the OLR, the pattern catches up with and passes through the material. Consider a two-armed spiral pattern. At the Lindblad resonances,

$$\Omega_p = \Omega \pm \kappa/m, \quad (2)$$

where  $\kappa$  is the epicyclic frequency, the  $+$  sign refers to OLR, the  $-$  sign to ILR, and  $m$  is the number of spiral arms. (Only two-armed spirals will be considered in this paper.) Figure 1 shows graphs of angular frequencies computed for a flat rotation curve.  $\Omega - \kappa/2$  is a decreasing function exterior to the ILR.

Let  $R_1$  be the innermost and let  $R_2$  be the outermost measured radii of the spiral structure.  $R_2 \leq R_{\text{CR}}$  implies

$$(\Omega - \kappa/2)_{\text{ILR}} = V/R_{\text{CR}} \leq V/R_2. \quad (3)$$

The epicyclic frequency is (e.g., Binney & Tremaine 1987)

$$\kappa(R) \equiv \left[ 2 \frac{V}{R} \left( \frac{dV}{dR} + \frac{V}{R} \right) \right]^{1/2}, \quad (4)$$

and for a flat rotation curve,

$$\kappa = \sqrt{2}V/R. \quad (5)$$

Equations 3 and 5 lead to

$$R_{\text{ILR}} \geq (1 - \sqrt{2}/2)R_2. \quad (6)$$

Since  $R_{\text{ILR}} \leq R_1$ , equation 6 implies

$$(1 - \sqrt{2}/2)R_2/R_1 \leq 1 \quad (7)$$

is the test of whether the observed spiral structure could fit between the ILR and CR. See §2.2 for necessary modifications and interpretation of equation 7 when the rotation curve is not flat. The numerical coefficient in equation 7 was referred to in §2 as the “typical” ratio.

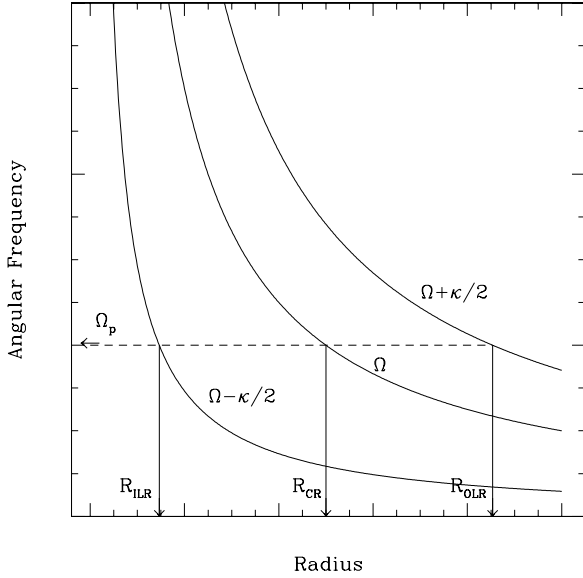


Fig. 1.— Schematic showing angular frequencies (in arbitrary units) for a flat rotation curve. Angular rotation frequency is  $\Omega$  and the epicyclic frequency is  $\kappa$ . The pattern “speed” is  $\Omega_p$ . Corotation resonance (CR) and inner (ILR) and outer (OLR) Lindblad resonances are marked.

What is the characteristic of spiral structure bounded between the ILR and OLR?  $R_{\text{ILR}} \leq R_1$  implies that

$$(\Omega - \kappa/2)_{R_1} \leq (\Omega - \kappa/2)_{\text{ILR}} = V/R_{\text{CR}}. \quad (8)$$

Equations 8 and 5 imply that

$$R_{\text{CR}} \leq (2 + \sqrt{2})R_1. \quad (9)$$

Since  $R_2 \leq R_{\text{OLR}}$ ,

$$(\Omega + \kappa/2)_{R_2} \geq (\Omega + \kappa/2)_{\text{OLR}} = V/R_{\text{CR}}. \quad (10)$$

Then equations 5 and 10 imply

$$(2 - \sqrt{2})R_2 \leq R_{\text{CR}}. \quad (11)$$

Combining equations 9 and 11 leads to the condition

$$R_2/(3 + 2\sqrt{2})R_1 \leq 1. \quad (12)$$

## 2.2. Other rotation curves

How does the shape of the rotation curve change the results of §2.1? Four functional forms for rotation curves will be explored. Rotation curves that are not strictly flat lead to numerical coefficients somewhat different than, but still close to, those in equations 7 and 12, so small violations of equations 7 or 12 are expected.

A rotation curve that is linearly rising or falling (having functional form  $V(R) = a + bR$  for  $a \neq 0$  and  $b$  small) will alter the values of the “typical” resonance ratios (equation 7 or equation 12). The changes are generally small and are independent of the value of  $a$ . Figure 2a shows the variation of the  $R_{\text{CR}}/R_{\text{ILR}}$  and  $R_{\text{OLR}}/R_{\text{ILR}}$  ratios for  $b = \pm 10\%(a/10 \text{ kpc})$ . The  $R_{\text{CR}}/R_{\text{ILR}}$  curve is asymptotic to  $\rho_7 \equiv 2 + \sqrt{2}$  and the  $R_{\text{OLR}}/R_{\text{ILR}}$  curve is asymptotic to  $\rho_{12} \equiv 3 + 2\sqrt{2}$ , diverging strongly only for very low pattern speeds.

Consider the following family of rotation curves:

$$V(R) = \frac{aR}{1 + bR}, \quad (13)$$

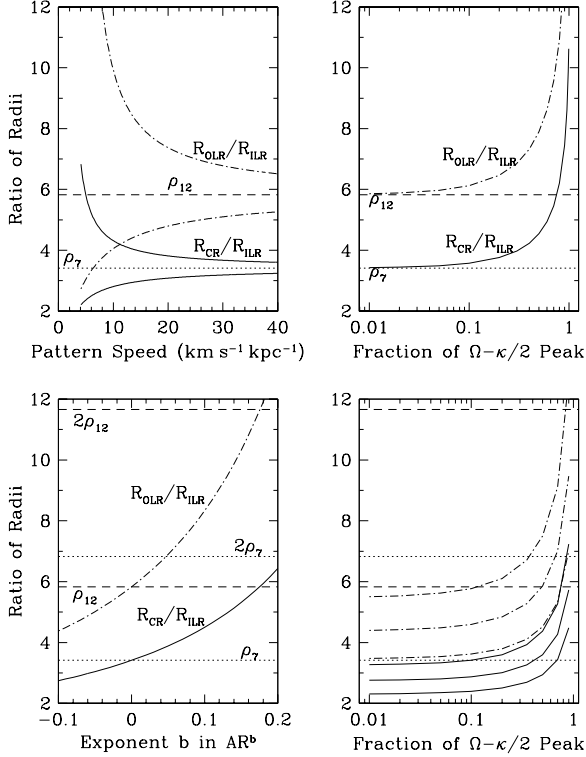


Fig. 2.— Graphs of the resonance ratios  $R_{CR}/R_{ILR}$  (solid lines) and  $R_{OLR}/R_{ILR}$  (dot-dash lines) for four rotation curve shapes: (a) linear rising (upper) or falling (lower) with slope 10% over 10 kpc; (b) equation 13 family; (c) power law; (d) three members of the equation 17 family with  $c = -0.01$  (upper),  $-0.02$  (middle), and  $-0.1$  (lower).  $\rho_7 = 2 + \sqrt{2}$ , from equation 7, and  $2\rho_7$  are shown by dotted lines.  $\rho_{12} = 3 + 2\sqrt{2}$ , from equation 12, and  $2\rho_{12}$  are shown with dashed lines. The pattern speed is represented in panels (b) and (d) by its value as a fraction of the peak in  $\Omega - \kappa/2$ .

where  $V(R)$  is the rotation speed as a function of radius  $R$  and  $a$  and  $b$  are free parameters. For small  $R$ ,  $V \sim aR$  is approximately linear, and for large  $R$ ,  $V \sim a/b$  is approximately constant, thus approximating the shapes of many real rotation curves.

Graphs of the ratios  $R_{CR}/R_{ILR}$  and  $R_{OLR}/R_{ILR}$  are shown in Figure 2b for the equation 13 family. The ratios are independent of the asymptotic rotation speed and the slope of the inner part. The ratios depend weakly on pattern speed until the pattern speed is a significant fraction (over 50%) of the value at the peak of the  $\Omega - \kappa/2$  curve. The curvature of the  $\Omega - \kappa/2$  curve (see Figure 3) pulls the ILR to a smaller radius than for a flat rotation curve. The smaller inner radius, used as the divisor in equation 7 or equation 12, will cause the computed value exceed unity. For the equation 13 rotation curves, the equation 7 value reaches 1.71 when the pattern speed is 75% of the angular frequency at the peak in  $\Omega - \kappa/2$ . (When the equation 7 value is 1.71, the equation 12 ratio is unity.) The equation 7 ratio equals 2 when the pattern speed is at 86% of the angular frequency at the peak. If the pattern speed exceeds the value at the peak, then there is no ILR, and spiral structure may (in principle) extend to the center of the disk. Then the  $R_{CR}/R_{ILR}$  and  $R_{OLR}/R_{ILR}$  ratios can be arbitrarily large.

Equations 7 and 12 will be called the “canonical” tests; replacing the unit value of the inequality by 2 will be called the “conservative” tests. When the conservative equation 7 test is applied, we are protecting ourselves against the case (a “false positive”) of a galaxy with a non-flat rotation curve giving a false indication that its CR is within its bright optical disk.

The power law is another family of rotation curve forms:

$$V(R) = aR^b. \quad (14)$$

Many dwarf galaxies and a moderate fraction of low surface brightness disk galaxies have rotation curves that are well approximated by a power law out to the farthest observed radius (de Blok,

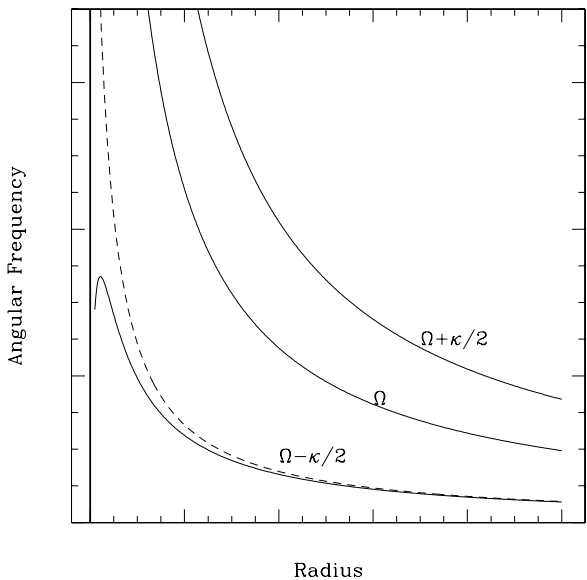


Fig. 3.— This figure is similar to Fig. 1 but displays angular frequency curves (solid lines) for a representative member of the equation 13 family. The dashed line shows for comparison the graph of  $\Omega - \kappa/2$  for a flat rotation curve with the same asymptotic rotation speed. A vertical solid line is drawn at zero radius.

McGaugh, & van der Hulst 1996; Pickering et al. 1997). Current thinking on galaxy formation suggests that rotation curves that have an inner power-law form will flatten out at larger radius (Dalcanton, Spergel, & Summers 1997). But it is nonetheless worth while to derive the resonance ratio tests when the rotation curve is a power law, since it is possible that the ILR and OLR are within the power law-like region of the rotation curve.

Rising rotation curves are given by positive values of the exponent  $b$ , with small values approximating a flat rotation curve; slowly falling but nearly flat curves are given by negative values of the exponent  $b$ . For power law rotation curves,

$$R_{\text{CR}}/R_{\text{ILR}} = \left[ 1 - \sqrt{(b+1)/2} \right]^{1/(b-1)}. \quad (15)$$

and

$$R_{\text{OLR}}/R_{\text{ILR}} = \left[ 2 \left( 1 - \sqrt{(b+1)/2} \right)^2 / (1-b) \right]^{1/(b-1)}. \quad (16)$$

Graphs of the variation of these ratios with exponent  $b$  are shown in Figure 2c. Although the ratios are a bit smaller than the canonical test values (equations 7 and 12) for the smallest reasonable values of  $b$ , the range between the canonical test value and the conservative test value includes most of the variation of the ratio graphs.

Consider finally the hybrid form (Elmegreen & Elmegreen 1990):

$$V(R) = aR / \left[ R^b + R^{(1-c)} \right]. \quad (17)$$

Some examples of rotation curves of this shape are shown in Fig. 4 in Elmegreen & Elmegreen (1990). Numerical solution for the resonance ratios led to the curves graphed in Figure 2d. In this case, too, the range between the canonical test value and the conservative test value includes much of the variation in the resonance ratios shown in Fig. 2d.

In all cases of realistic rotation curve shapes examined above, most of the variation in the resonance ratios falls within the range between the canonical and conservative tests derived for a flat rotation curve. For many rotation curves, the ratio is smaller than that for a flat rotation curve (see, e.g., Fig. 2*d*). The consequence of small ratios is that some interesting candidates may not be noticed. Galaxies with such rotation curves might have only a modest extent of spiral structure as measured by the canonical test, yet the extent of spiral structure could be near the maximum allowed by the location of the Lindblad resonances. Such a galaxy would be missed by the test proposed here. Although this circumstance decreases the efficiency of identifying promising galaxies, it also decreases the likelihood of incorrectly selecting a galaxy that does not, in fact, have its CR within its bright disk.

### 2.3. Other caveats

In a private discussion, A. Toomre noted potential problems that might result by assuming a unique pattern speed for the spiral structure, as was done in §§2.1-2.2. It is possible that the spiral structure is produced from spiral density waves with a range of pattern speeds about a well-defined characteristic pattern speed. There would then be both a general broadening of the observed pattern and an apparent penetration of the Lindblad resonances of the characteristic pattern. This effect can be seen in Fig. 8 of Toomre (1981), a classic illustration of a swing amplified spiral density wave, where the inner parts of the spiral become tightly wrapped and appear to penetrate the ILR. The model was constructed from spiral density wave packets with a Gaussian distribution of pattern speeds. To avoid the pitfalls of a spread of pattern speeds, only clearly defined spiral structure was measured for this paper, letting the seeing blur any high frequency interior structure, which was ignored.

In contrast, spiral structure that is a mode of the disk may have a single pattern speed, as will

spiral structure produced through swing amplification of a groove mode. In these cases, apparent extension of the spiral structure through Lindblad resonance should not be apparent.

### 3. Observations

CCD frames have been obtained for 140 galaxies. The observations span the period 1993 August 12 to 1997 September 7. All observations were made using the U.S. Naval Observatory 1 m telescope with any of four CCD detectors: either of two Texas Instruments 800<sup>2</sup>-pixel CCD's (the so-called "Banana" and "Flat" chips), a Tektronix 1024<sup>2</sup>-pixel CCD, or a Tektronix 2048<sup>2</sup>-pixel CCD. The image scale was 0.43 arcsec/pixel for the TI chips and 0.68 arcsec/pixel for the Tektronix chips. All the observations reported here were during nights that were photometric or that had light cirrus at worst; all frames reach comparable photometric depth. Seeing ranged from 1.4-3 arcsec full width at half maximum. Total exposure times were 30 minutes for all regular two-armed spiral galaxies except for the following: NGC4321 (40 minutes), ESO437-G044 (60 minutes, but very large zenith distance), NGC3054 (40 minutes), and NGC3433 (40 minutes). In cases where the nucleus was inordinately bright, two or more shorter exposures were stacked. All exposures used a Johnson *V*-band filter to attain large contrast in the spiral structure with reasonable exposure time.

Two classes of galaxies make up the observing list: physically large spirals and grand design spirals. Because rotation curves of spirals are usually flat, physically large spirals have a good chance of having spiral structure so extensive that the CR is within the bright disk. The enormous galaxy UGC02885 (Roelfsema & Allen 1985; Canzian, Allen, & Tilanus 1993) is the archetype of this class. (If rotation curves were usually linearly rising, instead of flat, then the scale-free form of a logarithmic spiral would not favor any particular size of spiral galaxy for this investigation.) Data from the litera-

ture were processed to find physically large spiral galaxies. Contributing to the list are observations by Baiesi-Pillastrini (1983); Bica & Giovanelli (1986a,b, 1987); Freudling, Haynes, & Giovanelli (1988); Giovanelli & Haynes (1985a,b, 1989, 1993); Giovanelli et al. (1986); Gordon & Gottesman (1981); Haynes & Giovanelli (1984, 1986, 1991); Haynes et al. (1988); Hewitt, Haynes, & Giovanelli (1983); Huchtmeier & Richter (1989); Kyazumov (1984); Lewis (1985); Nilson (1973); Romanishin (1983); Sandage & Tammann (1981); Scaglia & Sancisi (1988); Schneider et al. (1986); Scodreggio & Gavazzi (1993); Stavely-Smith & Davies (1988); de Vaucouleurs, de Vaucouleurs, & Corwin (1976); Wegner, Haynes, & Giovanelli (1993). Table 1 lists the 50 largest spiral galaxies assembled from the above sources. An index of physical size, the product of Doppler velocity and angular size, was used to rank the galaxies. The same galaxy reported in several sources will appear several times in the list from which Table 1 was culled. In most cases, the several entries for the same galaxy were not wildly separated in the ranked list. Table 2 lists the 50 largest spiral galaxies in the RC3 (de Vaucouleurs et al. 1991), a homogeneous catalog. (In Table 2, the velocity is with respect to the 3K background.) Tables 1 and 2 include only spirals with morphological type between Sb and Sc (inclusive) to help ensure enough HI for emission line mapping (if desired) and to avoid the ragged spiral structure of Sd and later types. (The analysis of §§2.1-2.2 does not apply to multiple-armed or flocculent spirals.) Sometimes the literature source only specified that the object was a spiral (morphological type “S”), usually because the object was too distant to show enough structure to determine a Hubble subtype. Such cases were permitted in the observing list because the source material may have been poor and a much better CCD frame could reveal more structure. In addition, the inclination of the galaxy was restricted to be in the range  $27^\circ$  to  $68^\circ$ , based on major and minor axis angular sizes, so that the spiral struc-

ture would be clear and later kinematic analysis would be possible. Many of the galaxies in Tables 1 and 2 were observed as part of the observing program reported in this paper.

Grand design spirals of all sizes were sought in addition to the physically large spirals. Objects from Elmegreen et al. (1987) with arm class 12 (“grand design”) were chosen in addition to objects whose photos in atlases (Sandage & Bedke 1988; Sandage & Tammann 1981; Wray 1988) showed clear two-armed grand design spiral structure.

Table 3 shows the final list of objects observed with brief comments about their spiral structure. Two-armed grand design spirals (called “2-arm g.d.” in Table 3) may have spurs or feathers that are not so prominent as to give the disk a multiple arm appearance. Spiral structure that is “not regular” may have arms with wildly varying pitch, there may be more than one pattern, or some other deviation from two-armed grand design structure. Galaxies marked “faint” lack enough signal in the exposure to categorize the spiral structure.

Limited morphological information that is useful to the discussion in §5 is also reported in Table 3. The presence of a bar is denoted by the symbol “B”; an inner ring is denoted by “r” and an inner pseudoring by “p”; an outer ring is denoted “R” and an outer pseudoring by “P”. (I apologize to Ron Buta for this abbreviated classification scheme.) If the galaxy is not barred, it is designated “S”. When the feature is not clear, the symbol is followed by a “.”. Deprojection (which elongates round features) may cause uncertainty about the presence of a bar. The presence of a bar is also uncertain when the galaxy has an S-shape: then it is not clear if the nearly straight central segment is a bar or merely the convergence of two open spiral arms on the nucleus. Inner rings may be round or pointy (that is, lozenge-shaped). Pseudorings are ring-like features that appear to be formed by spiral arms, and may or may not be closed. (See Buta 1986 on



the morphology of rings and pseudorings.) Inner pseudorings usually have a lozenge shape and are generally not closed. The distinction between an inner pseudoring and a pointy inner ring is not clear. For this paper, if the spiral arms followed continuously from the ring segments, or if the ring segments did not close, then the feature was called a pseudoring. If the ring segments were closed and the spiral arms were not obviously extensions of the segments, then the feature was called an inner ring. Outer pseudorings have a fat dumbbell or figure-eight shape.

#### 4. Analysis

A downhill simplex algorithm (Press et al. 1988) fitted ellipses to isophotes by minimizing the isophotal deviations around the ellipses. The apparent shape of the disk was characterized by the outer isophotes, which then specified the deprojection of the image. Deprojection was done with IRAF (Image Reduction and Analysis Facility). Table 3 lists the position angles and inclinations (to the nearest degree) used for the deprojection. Indeterminate position angles result when the inclination is small. The table lists formal errors on position angle and inclination that were computed from the fitting errors of ellipses that characterize the outer isophotes. The fitting errors were empirically derived by varying the starting point in parameter space for the downhill simplex algorithm and compiling the deviations among the ending points.

The radial extent of spiral structure was measured on deprojected images of the galaxies. The inner and outer extent of the spiral structure was marked conservatively, given the caveats in §§2.2–2.3. (Inner spiral structure had to be clear; outer spiral structure had to have reasonable signal-to-noise, described below.) The inner and outer radii of spiral structure for the two-armed grand design spirals are listed in Table 4. Some galaxies show two patterns: they have faint spiral structure in their outer disks that is of a different character than the bright inner arms (see

Elmegreen & Elmegreen 1995 on this topic). For galaxies with an inner and an outer pattern, separate computations were made for the end of the bright spiral pattern and the end of its faint extension.

The column in Table 4 labeled “S/N” indicates the signal-to-noise ratio for the outer spiral structure detection. Signal was measured as a  $7 \times 7$ -pixel ( $5'' \times 5''$ , a typical spiral arm width for galaxies observed here) average within the spiral arm at the furthest extent of the spiral structure. Local sky was determined from an average of four such  $7 \times 7$ -pixel averages in nearby, almost emission-free areas. The noise was determined as the average standard deviation from the mean in the four sky measurements.

Surface photometry in the literature was used to calibrate the instrumental surface brightness profiles of some galaxies. The effect of foreground stars on the measured profiles was reduced by ignoring the brightest 10% of the pixels in each radial zone. Ignoring bright pixels is admittedly not as accurate as fitting stellar profiles and subtracting stars from each frame. The object of this exercise is not to derive accurate surface photometry, however, but rather to measure the photometric depth of the data frames.

The calibrated surface brightness profiles are shown in Figure 4. There is excellent agreement in detail with most profiles from the literature. Small discrepancies in limited radial ranges can be attributed to the effects of foreground stars that were not uniformly treated in all published surface brightness studies. Surface brightness profiles are typically reliable to about  $27 \text{ mag arcsec}^{-2}$ . At this isophotal level, the signal-to-noise ratio (S/N) has dropped to 2.5, counting signal within a typical seeing disk (about  $2 \text{ arcsec}$ ).

The surface brightness at which the outer extent of spiral structure was determined was typically much brighter than  $27 \text{ mag arcsec}^{-2}$ . Using the calibrated surface photometry shown in Fig. 4 and outer spiral extents from Table 4,

the mean surface brightness at the outer extent of the spiral structure was computed (Table 5). Spiral arms are significantly brighter than the mean surface brightness, though. Given that the gain of the Tek1K chip (the most frequently used detector for this study) is  $7.4 e^- \text{ pix}^{-1}$ , its read noise ( $6 e^-$ ) is insignificant compared to sky noise for 30-minute exposures, and that the mean sky brightness at the U. S. Naval Observatory Flagstaff Station at  $V$ -band is  $21.5 \text{ mag arcsec}^{-2}$ , the S/N per pixel equals unity for the  $26 \text{ mag arcsec}^{-2}$  isophote. Probably the brightness of the spiral arm at the outer spiral extent reported in Table 4 can be, at faintest, about  $26 \text{ mag arcsec}^{-2}$  at  $V$ -band. Note that the surface brightness at the outer extent of the spiral structure can be much brighter if, for instance, only the extent of the bright, inner arms is reported in Table 4 (e.g., for NGC0521).

Given the generally large values of S/N at the outer spiral extent listed in Table 4 and the fact that the data frames are rather deep (as shown by the surface photometry in Fig. 4), nearly all the optically luminous spiral structure is recorded on the data frames and generally it is recorded comfortably above the noise threshold of the frames.

The results of checking for violations of equation 7 and adherence to equation 12 are shown in Table 4 for the grand design spirals. Violations are assessed according to the “conservative” tests (§2.2). A “dot” in the “Pass?” column indicates that the conservative test is passed with a measured value of the ratio less than 1.71; a “ $\sim$ ” in the “Pass?” column indicates a value of the ratio from 1.71 to 2.0; and if the measured ratio is over 2.0, there is an “N” in the “Pass?” column, indicating a violation of the conservative ratio test.

## 5. Discussion

The distribution of values of the equation 7 and equation 12 ratios is shown in Figure 5. Only a single increment is shown for each galaxy in Ta-

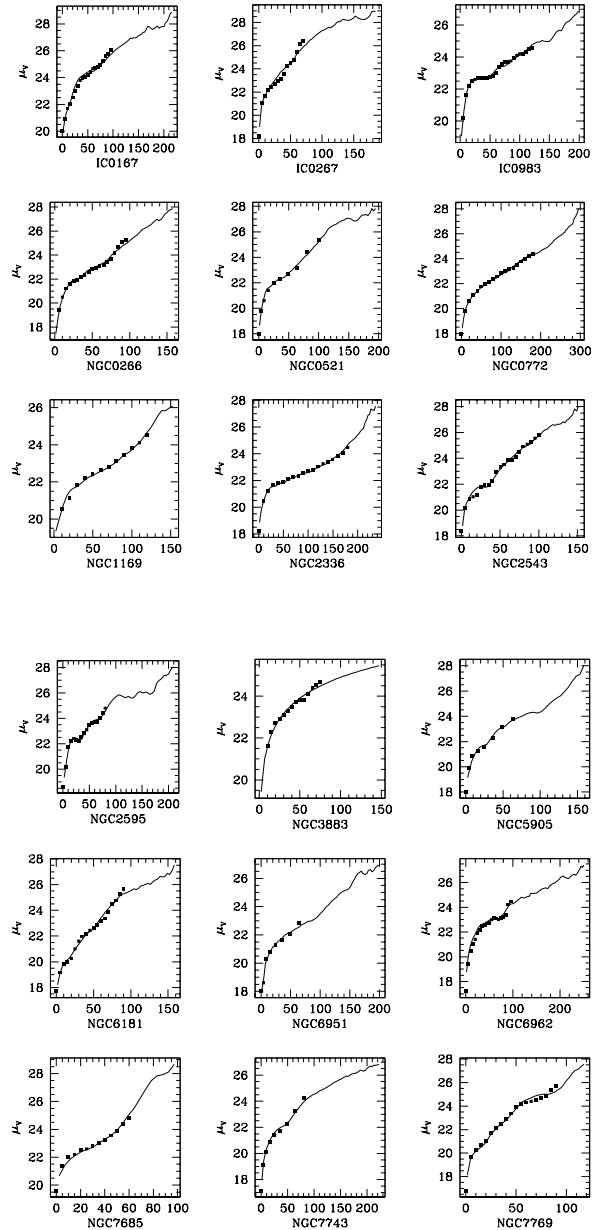


Fig. 4.— These are calibrated surface brightness profiles for some galaxies in the survey. Surface brightness in  $V \text{ mag arcsec}^{-2}$  is graphed versus radius in arcseconds. The filled squares are data from the literature. The lines are the calibrated surface brightness profiles from CCD imaging observations reported here, which are reliable to about  $27 V \text{ mag arcsec}^{-2}$ .

ble 4, except that NGC5248 and NGC6632 have two contributions because these galaxies have two distinct spiral patterns. In other cases where there are two entries for the same galaxy in Table 4, the entry that represented the most extensive, continuous, two-armed spiral structure was chosen. Ratios corresponding to the extent of extra or detached arms are not illustrated in Fig. 5.

Most of the galaxies have values of the equation 12 ratio that are less than unity. This observation is consistent with spiral density wave theory (spiral structure bounded by the Lindblad resonances) and the fact that most rotation curves are approximately flat. Effects due to the shape of the rotation curve (§2.2) can explain the few ratios larger than unity.

Surprisingly many grand design spirals have small values of the equation 12 ratio (peaked around 0.3 in Fig. 5). Can theories of the creation of grand design spiral structure explain this preponderance of low values? Swing amplification (see, e.g., Toomre 1981) of disturbances created by companions (Byrd & Howard 1992) or a groove (Sellwood & Kahn 1991) should create spirals that reach both their ILR and OLR. If the swing-amplified spiral is a superposition of spiral density waves with a range of pattern speeds (§2.3), then measurement of the extent of the spiral could lead to an equation 12 ratio greater than unity, not less. But under modal theory (see, e.g., Bertin et al. 1989a,b), the innermost extent of the spiral would be the  $Q$ -barrier, which is exterior to the ILR, thus decreasing the equation 12 ratio.

The best explanation for the low values of the equation 12 ratio involves the resonant interaction of spirals with bars and rings, as will be discussed below. There is a peak in the distribution of values of equation 7 near 0.5 (see Fig. 5). Most of the galaxies contributing to the peak are barred and ringed galaxies.

The distributions of the values of the equation 7 ratio are graphed separately in Figure 6 for

three morphological classes: pure spirals with no sign of ring or bar, barred galaxies (which may have a ring), and ringed galaxies (which may also have a bar) including galaxies with pseudorings. Galaxies showing signs of strong interaction, such as an anomalously long spiral arm and a probable companion, were omitted from all the distributions. For example, galaxies resembling Arp 82 or Arp 248, which have long and obvious tidal tails, were excluded from the distributions. Galaxies resembling M51, which show a close interaction but no tidal tails, were excluded because the projection of a tidal tail nearly along the line of sight could masquerade as a spiral arm in such cases. Galaxies resembling M81 were included in the distributions. Although M81 has spiral structure that resulted from an interaction with a companion, its spiral structure is a spiral density wave in the disk and there is no sign of a tidal tail or other structure out of the plane of the disk. The galaxies in Table 4 that were excluded from the distributions are Anon0958–14, ESO437–G044, IC0167, IC1551, IC2421, NGC0280, NGC2535, NGC4321, NGC7753, NGC7769, UGC04457, UGC11453, and UGC11695.

As in Fig. 5, when two ratio values are listed in Table 4, the entry corresponding to the main two-armed spiral structure is included in the Fig. 6 histogram. In a few cases where the uncertain morphology could move a galaxy from the barred or ringed class to the pure spiral class (for instance “B:” might be “B” or “S”, and “r:” might be “r” or “S”), the galaxy is graphed on histograms for both possible classes as an unshaded box.

The values of the equation 7 ratio are much more evenly distributed for pure spirals than they are for the other morphological classes. (Pure spirals comprise less than one-third of the sample, making their statistics somewhat noisier than those for barred or ringed galaxies.) The distributions of the equation 7 ratio for barred and ringed galaxies, in contrast to pure spirals,

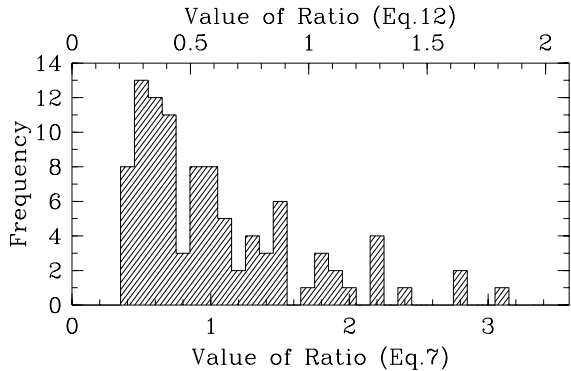


Fig. 5.— Here are distributions of the equation 7 (lower scale) and equation 12 (upper scale) ratios for qualified galaxies from Table 4.

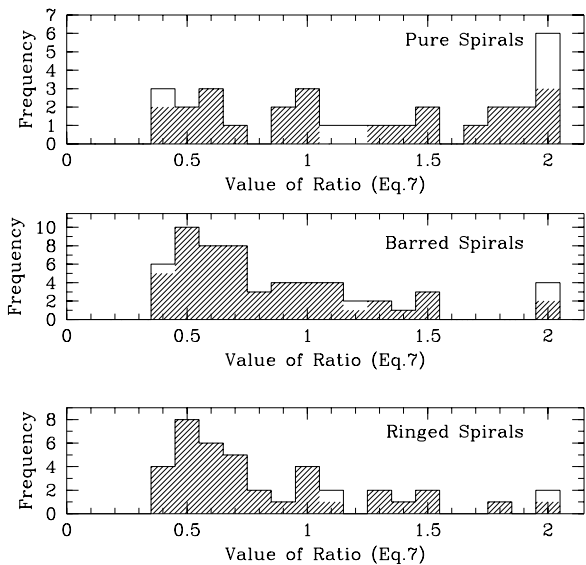


Fig. 6.— The distribution of the equation 7 ratios are graphed here separately for pure spirals, barred spirals, and ringed spirals. Uncertain morphologies are graphed as an unshaded increment in the two appropriate panels. Barred spirals with rings contribute to two panels.

are decidedly peaked at small values (around 0.5 to 0.7). The different appearance of the distributions in Fig. 6 can be quantified by a Kolmogorov-Smirnov test (cf. Press et al.). The probability that the ratios for pure spirals are drawn from the same population as those for the barred spirals is less than 1%; the probability is just over 1% for pure and ringed spirals. In contrast, the ratios for barred and ringed spirals have a 97% probability of being drawn from the same population. The last statistic is not surprising, since many galaxies have both bar and ring features. (Over half the barred galaxies in this study are also ringed.)

A correlation between limited spiral extent and the presence of a bar can be explained if, in many barred spirals, the bar and spiral are resonantly related. Modeling of barred spirals indicates that strong bars end at or just short of their CR (Contopoulos 1980; cf. also Elmegreen 1996). If the spiral patterns in strongly barred spirals had the same pattern speed as the bar, then spirals could extend only between their CR and OLR. For such a barred spiral, the equation 12 ratio would be  $(1 + \sqrt{2}/2)/(2 + \sqrt{2}) = 0.5$ .

All bars are not strong, though. The relationship, if any, between the end of a weak bar and its resonances is not known. Furthermore, it is not established that bars and spirals are resonantly related when they appear together in the same galaxy. So the rationale explaining why galaxies with bars tend to have less extensive spiral structure may be only a partial explanation. The explanation may be true often enough, however, to explain why there is a peak around 0.5–0.7 in Fig. 6 for barred spirals but no peak for pure spirals.

A correlation between limited spiral extent and the presence of an inner ring can also be explained if, as is fairly well established, inner rings are resonance phenomena. Inner rings and pseudorings seem to be located at the inner 4:1 resonance (cf. Combes 1996), which is exterior to the ILR. Limiting spiral structure to the range

between inner 4:1 and OLR also decreases the equation 12 ratio.

Other aspects of rings are neutral to the discussion or are problematic. The location of an outer ring at the OLR (Buta & Crocker 1991) does not place an extra limitation on spiral extent, and so does nothing to decrease the equation 12 ratio. Many barred spirals also have an inner ring circumscribing the bar. It is not clear if it is possible to reconcile the presence of a strong bar (ending inside its CR) with a surrounding inner ring (at the 4:1 resonance), although a weak bar and inner ring might be possible.

### 5.1. Particular galaxies

Descriptions of the spiral structure of two-armed grand design spiral galaxies with the largest values of the resonance ratios follow below, where the relative merit of each galaxy for kinematic or resonance analysis is assessed. Because the shape of the rotation curve is not known, the inclusion of a galaxy in this list is no guarantee that the CR for the two-arm spiral pattern is within the optical disk (see §2.2).

*NGC5829.* This galaxy appears to be a member of a small group (HCG73: Hickson, Kindl, & Auman 1989). One apparent member of the group shows signs of recent interaction (tidal tail or one-armed spiral emerging from an off-center, nucleated, disturbed or irregular galaxy). Spiral structure reaches a very small radius, leading to a large equation 7 ratio. There is some danger that the outer disk is distended or not planar owing to encounters within the group.

*NGC6907.* This galaxy may have a central oval, although the morphology of the spiral arms may contribute to the illusion of the oval. In the inner disk, spiral structure is bright and sharply defined, with regions of dust and star formation. In the outer disk, spiral arms are faint, smooth, and broad. One spiral arm wraps through considerably more phase than the other.

*IC0211.* Spiral structure penetrates to very small radius in this galaxy. The arms are somewhat faint and diffuse, although they are lightly dappled with regions of star formation.

*NGC1042.* Much of the spiral structure of this galaxy is faint, diffuse, and punctuated by bright knots (thus resembling IC0211). The spiral structure in the inner disk consists of two short, bright arcs.

*UGC10104.* The inner disk has very regular, two-armed spiral structure. There is a radial gap at the end of one bright inner arm, followed by a fainter, more diffuse, somewhat fragmentary outer arm. The other bright inner arm shows similar behavior, except that the corresponding outer arm tracks the outer rim of the inner arm for about 30 degrees in azimuth before the inner arm fades. It is possible that there are two resonantly related two-armed spiral patterns in this galaxy. If so, then the ratio reported in Table 4 is inappropriately large.

*NGC0132.* This galaxy may have a central oval, or else (like NGC6907) the inner spiral arms mimic a lozenge shape. One arm has a ragged and feathery appearance.

*NGC0173.* The spiral structure in the inner disk has a feathery appearance and it is somewhat difficult to trace the arms continuously into the outer disk. The spiral arms in the outer disk are narrow and dotted by regions of star formation.

*NGC7685.* The spiral structure is somewhat feathery and is complicated by the emergence of a short arm from the interarm region between the two main spiral arms.

The following galaxies marginally pass the conservative test (indicated by a “~” in Table 4).

*UGC04643.* The spiral structure is very regular and winds through a turn and a half. The arms make an abrupt transition from bright to faint after about a full turn. The spiral arms in the outer disk are still rather narrow and are not diffuse, in contrast to other galaxies with differ-

ent arm brightnesses in the inner and outer disk.

*UGC09808.* The spiral arms are exceptionally thin. There is some irregularity in the emergence of the two-armed spiral. It appears that there is a single spiral arm in the inner disk that leads continuously, except for a kink or cusp, to one of the two main outer arms. The second main arm emerges in a manner symmetrical to the first, but without obvious connection to the inner disk. A short arm or arc emerges from the interarm region interior to the main arm with the kink. The short arm is initially bright but quickly dims and broadens. Both of the main arms make a transition from narrow and bright to fainter and more diffuse in the outer disk.

*NGC3897.* The spiral arms are narrow and emerge from nearby the nucleus. The otherwise regular morphology is complicated by one arm forking in the outer disk. The inner tine of the forked arm winds a half turn into the outer disk as a broader, faint arm. The outer tine of the forked arm is initially the brighter tine but it fades after a quarter turn.

*IC2627.* This galaxy has two bright arms in the inner disk that abruptly and symmetrically transition to broader, faint arms in the outer disk. One of the main arms is considerably longer than the other. A very faint, third arm that winds half a turn in the outer disk emerges from an interarm region between the two main inner arms.

*NGC4079.* The spiral structure is very regular and winds inward to a rather small radius. There is an abrupt change from bright, narrow arms in the inner disk to broad, faint arms in the outer disk, suggesting a resonance crossing. This galaxy is an exemplary case for kinematic and resonance analysis. The author has obtained VLA HI data with which to map its velocity field.

## 6. Conclusions

This paper describes an observational project that examined 140 spiral galaxies, measuring the visual extent of their spiral structure. The purpose of the project was to find galaxies for which the corotation resonance of the two-armed grand design spiral structure was likely to be within the bright optical disk. The likelihood that the corotation resonance is within the optical disk can be assessed by comparing the measured ratio of outer to inner spiral extent with the value of the canonical ratio (equation 7).

The test using the canonical ratio is not conclusive because of variations due to rotation curve shape. It is also possible that there is no inner Lindblad resonance. To counter our ignorance of the rotation curve, a test with a more conservative value of the ratio than equation 7 should be used (here, an extra factor of two).

A few galaxies were found that have large spiral extent and whose corotation resonance radius is very likely to be within the bright optical disk. Among the best candidates for kinematic study are NGC5829, NGC6907, IC0211, NGC1042, and NGC0132.

It was incidentally found that barred and ringed spirals statistically have more limited spiral extent than pure spirals. This observation can be explained if many bars end at their inner 4:1 or corotation resonance and if the bar and spiral are part of the same pattern. The location of inner rings at the inner 4:1 resonance also limits spiral extent, but the location of outer rings at the outer Lindblad resonance places no extra constraint on spiral extent.

This research was supported in part by the Director's Research Fund at the Space Telescope Science Institute. I thank Otto Richter for an electronic copy of his table of HI observations and Riccardo Giovanelli for electronic copies of several tables summarizing HI observations. I have benefited from conversations

with Ken Freeman, Piet van der Kruit, and Alar Toomre. Arne Henden kindly observed and provided processed CCD frames of six of the galaxies for this project. Thanks to the referee, Bruce Elmegreen, for his comments and criticisms that led to improvements of this paper. Provisional images of some galaxies were obtained during a preliminary phase of this research using the Guide Stars Selection System Astrometric Support Program developed at the Space Telescope Science Institute (STScI is operated by the Association of Universities for Research in Astronomy, Inc. for NASA). This research has made use of the NASA/IPAC Extragalactic Database (NED), which is operated by the Jet Propulsion Laboratory, Caltech, under contract with the National Aeronautics and Space Administration. Electronic copies of several tables of galaxy and redshift information were obtained from the National Space Science Data Center and the Astronomical Data Center.

## REFERENCES

- van Albada, G. D., & Roberts, W. W., Jr. 1981, *ApJ*, 246, 740
- Baiesi-Pillastrini, G. C. 1983, *A&AS*, 53, 373
- Bertin, G., Lin, C. C., Lowe, S. A., & Thurstans, R. P. 1989a, *ApJ*, 338, 78
- Bertin, G., Lin, C. C., Lowe, S. A., & Thurstans, R. P. 1989b, *ApJ*, 338, 104
- Bicay, M. D., & Giovanelli, R. 1986a, *AJ*, 91, 705
- Bicay, M. D., & Giovanelli, R. 1986b, *AJ*, 91, 732
- Bicay, M. D., & Giovanelli, R. 1987, *AJ*, 93, 1326
- Binney, J., & Tremaine, S. 1987, *Galactic Dynamics* (Princeton: Princeton University Press)
- de Blok, W. J. G., McGaugh, S. S., & van der Hulst, J. M. 1996, *MNRAS*, 283, 18
- Buta, R. 1986, *ApJS*, 61, 609
- Buta, R., & Crocker, D. A. 1991, *AJ*, 102, 1715
- Byrd, G. G., & Howard, S. 1992, *AJ*, 103, 1089
- Canzian, B., Allen, R. J., & Tilanus, R. P. J. 1993, *ApJ*, 406, 457
- Canzian, B., & Allen, R. J. 1997, *ApJ*, 479, 723
- Cepa, J., & Beckman, J. E. 1990, *ApJ*, 349, 497
- Combes, F. 1996, in *Barred Galaxies*, ed. R. Buta, D. A. Crocker, & B. G. Elmegreen (ASP Conf. Ser. vol. 91), 286
- Contopoulos, G. 1980, *A&A*, 81, 198
- Dalcanton, J. J., Spergel, D. N., & Summers, F. J. 1997, *ApJ*, 482, 659
- Elmegreen, B. G. 1996, in *Barred Galaxies*, ed. R. Buta, D. A. Crocker, & B. G. Elmegreen (ASP Conf. Ser. vol. 91), 197
- Elmegreen, B. G., & Elmegreen, D. M. 1990, *ApJ*, 355, 52
- Elmegreen, B. G., Elmegreen, D. M., & Montenegro, L. 1992, *ApJS*, 79, 37
- Elmegreen, B. G., Elmegreen, D.M., & Seiden, P. E. 1989, *ApJ*, 343, 602

- Elmegreen, D. M., & Elmegreen, B. G. 1987, *ApJ*, 314, 3
- Elmegreen, D. M., & Elmegreen, B. G. 1995, *ApJ*, 445, 591
- Freudling, W., Haynes, M. P., & Giovanelli, R. 1988, *AJ* 96, 1791
- Giovanelli, R., & Haynes, M. P. 1985a, *AJ*, 90, 2445
- Giovanelli, R., & Haynes, M. P. 1985b, *ApJ*, 292, 404
- Giovanelli, R., & Haynes, M. P. 1989, *AJ*, 97, 633
- Giovanelli, R., & Haynes, M. P. 1993, *AJ*, 105, 1271
- Giovanelli, R., Haynes, M. P., Myers, S. T., & Roth, J. 1986, *AJ*, 92, 250
- Gordon, D., & Gottesman, S. T. 1981, *AJ*, 86, 161
- Haynes, M. P., & Giovanelli, R. 1984, *AJ*, 89, 758
- Haynes, M. P., & Giovanelli, R. 1986, *ApJ*, 306, 466
- Haynes, M. P., & Giovanelli, R. 1991, *AJ*, 102, 841
- Haynes, M. P., Giovanelli, R., Starosta, B. M., & Magri, C. 1988, *AJ*, 95, 607
- Hewitt, J. N., Haynes, M. P., & Giovanelli, R. 1983, *AJ*, 88, 272
- Hickson, P., Kindl, E., & Auman, J. R. 1989, *ApJS*, 70, 687
- Huchtmeier, W. K., & Richter, O.-G. 1989, *A General Catalog of HI Observations of Galaxies* (New York: Springer-Verlag)
- Knapen, J. H., Beckman, J. E., Cepa, J., van der Hulst, J. M., & Rand, R. J. 1992, *ApJ*, 385, L37
- Knapen, J. H., Beckman, J. E., Cepa, J., & Nakai, N. 1996, *å*, 308, 27
- Kyazumov, G. A. 1984, *Sov. Astron.*, 28, 496
- Lewis, B. M. 1985, *ApJ*, 292, 451
- Lindblad, P. A. B., Lindblad, P. O., & Athanasoulas, E. 1996, *å*, 313, 65
- Nilson, P. 1973, *Uppsala General Catalogue of Galaxies* (Uppsala: Uppsala Offset Center AB)
- Pickering, T. E., Impey, C. D., van Gorkom, J. H., & Bothun, G. D. 1997, *AJ*, 114, 1858
- Press, W. H., Flannery, B. P., Teukolsky, S. A., & Vetterling, W. T. 1988, *Numerical Recipes* (Cambridge: Cambridge University Press)
- Roberts, W. W. 1969, *ApJ*, 158, 123
- Roelfsema, P. R., & Allen, R. J. 1985, *A&A*, 146, 213
- Romanishin, W. 1983, *MNRAS*, 204, 909
- Sandage, A., & Bedke, J. 1988, *Atlas of Galaxies Useful for Measuring the Cosmological Distance Scale* (NASA SP-496) (Washington, D.C.: U.S. Government Printing Office)
- Sandage, A., & Tammann, G. A. 1981, *A Revised Shapley-Ames Catalog of Bright Galaxies* (Washington, D.C.: Carnegie Institute of Washington Publication 635)
- Scaglia, R. P., & Sancisi, R. 1988, *A&A*, 203, 28
- Schneider, S. E., Helou, G., Salpeter, E. E., & Terzian, Y. 1986, *AJ*, 92, 742
- Schwarz, M. P. 1981, *ApJ*, 247, 77
- Scodreggio, M., & Gavazzi, G. 1993, *ApJ*, 409, 110
- Sellwood, J. A., & Kahn, F. D. 1991, *MNRAS*, 250, 278
- Sellwood, J. A., & Sparke, L. S. 1988, *MNRAS*, 231, 25p
- Sempere, M. J., Garcia-Burillo, S., Combes, F., & Knapen, J. H. 1995, *å*, 296, 45
- Stavely-Smith, L., & Davies, R. D. 1988, *MNRAS*, 231, 833
- Toomre, A. 1977, *ARA&A*, 15, 437
- Toomre, A. 1981, in *The Structure and Evolution of Normal Galaxies*, ed. S. M. Fall & D.



- Lynden-Bell (Cambridge: Cambridge University Press), 111
- de Vaucouleurs, G., de Vaucouleurs, A., & Corwin, H. G., Jr. 1976, Second Reference Catalogue of Bright Galaxies (Austin: University of Texas Press)
- de Vaucouleurs, G., de Vaucouleurs, A., Corwin, H. G., Jr., Buta, R. J. , Paturel, G., & Fouque, P. 1991, Third Reference Catalogue of Bright Galaxies (New York: Springer-Verlag)
- Wegner, P., Haynes, M. P., & Giovanelli, R. 1993, AJ, 105, 1251
- Wray, J. D. 1988, The Color Atlas of Galaxies (New York: Cambridge University Press)

TABLE 1  
LARGEST 50 GALAXIES (VARIOUS SOURCES)

$a \times V$	Name	Alt. Name	$a$ arcmin	$V$ $\text{km s}^{-1}$	Ref.
61875	Malin1		2.50	24750	(1)
40709	UGC02885		7.02	5799	(1)
36210	UGC08058	Anon1254+57	1.7	21300	(2)
34330	IC1551	UGC00268	2.6	13204	(3)
31292	IC0983	UGC09061	5.75	5442	(1)
30697	UGC11473		6.60	4651	(1)
29476	UGC10104	Anon1555+30	2.95	9992	(4)
26472	UGC02339		1.60	16545	(12)
25571	NGC3883	UGC06754	3.64	7025	(1)
25341	NGC5174	UGC08475	3.70	6849	(1)
25254	NGC5688		9.00	2806	(1)
25056	IC0226	UGC01922	2.30	10894	(1)
24488	NGC2206	UGCA123	3.90	6279	(1)
23870	UGC05813	UGC05813	1.8	13261	(3)
22631	UGC01886		4.50	5029	(11)
22523	NGC2713	UGC04691	5.75	3917	(1)
22464	UGC09515		1.6	14040	(5)
22198	NGC1241		5.50	4036	(1)
22128	UGC02151		2.0	11064	(8)
21755	UGC12128		1.1	19777	(10)
21725	NGC0772	UGC01466	8.86	2452	(1)
21577	NGC1961	UGC03334	5.50	3923	(1)
21122	IC1142	UGC10055	1.5	14081	(5)
21040	NGC1085	UGC02241	3.1	6787	(6)
20619	NGC5981	UGC09948	4.10	5029	(1)
20544	NGC2446	UGC04027	2.10	9783	(1)
20504	IC4381	UGC09073	2.20	9320	(1)
20477	UGC00520		1.00	20477	(12)
20222	NGC4939		6.50	3111	(1)
20122	NGC5619	UGC09255	2.4	8384	(7)
20075	NGC0497	UGC00915	2.5	8030	(2)
19958	UGC12084		1.6	12474	(9)
19839	UGC09025		1.10	18035	(1)
19497	Anon2233+34		2.95	6609	(1)
19345	NGC6007	UGC11079	1.82	10629	(4)
19180	NGC1530	UGC03013	7.80	2459	(1)
19166	NGC2336	UGC03809	8.70	2203	(1)
19164	IC0213	UGC01719	2.30	8332	(12)
19089	IC1173	UGC10180	1.83	10431	(1)
18985	NGC1169	UGC02503	7.95	2388	(1)

TABLE 1—*Continued*

$a \times V$	Name	Alt. Name	$a$ arcmin	$V$ $\text{km s}^{-1}$	Ref.
18946	NGC5172	UGC08477	4.70	4031	(1)
18921	NGC7753	UGC12780	3.5	5406	(8)
18795	UGC04457	Anon0829+19A	1.70	11056	(4)
18717	UGC10405		1.7	11010	(3)
18634	NGC5905	UGC09797	5.50	3388	(1)
18600	NGC0858		1.51	12318	(4)
18591	UGC01212		1.70	10936	(11)
18522	NGC3968	UGC06895	2.90	6387	(1)
18403	NGC0536	UGC01013	3.55	5184	(1)
18389	UGC09107		1.2	15324	(5)

NOTE.—(1) Huchtmeier & Richter (2) Nilson (3) Haynes & Giovanelli (1984) (4) de Vaucouleurs et al. (1976) (5) Freudling et al. (6) Kyazumov (7) Haynes & Giovanelli (1991) (8) Giovanelli & Haynes (1985a) (9) Giovanelli et al. (1986) (10) Giovanelli & Haynes (1989) (11) Wegner et al. (12) Giovanelli & Haynes (1993)

TABLE 2  
LARGEST 50 GALAXIES (RC3)

$a \times V$	Name	Alt. Name	$a$ arcmin	$V_{3K}$ $\text{km s}^{-1}$
32641	IC1551	UGC00268	2.57	12699
30509	IC0983	UGC09061	5.37	5681
28442	UGC02885		5.01	5675
27559	UGC04219		2.19	12597
26732	UGC10104	Anon1555+30	2.69	9932
23874	IC0226	UGC01922	2.24	10664
23306	UGC03139		3.72	6273
21677	NGC3883	UGC06754	2.95	7345
21156	UGC09234		1.91	11103
20745	UGC04457	Anon0829+19A	1.82	11400
20550	UGC09515		1.45	14217
20300	NGC1085	UGC02241	3.09	6569
20084	UGC12128		1.05	19180
19614	UGC03531		1.62	12094
19601	NGC1961	UGC03334	5.01	3911
19300	NGC4939		5.62	3432
19054	UGC02151		1.78	10715
18854	NGC5619	UGC09255	2.19	8618
18588	UGC03374		3.02	6155
18392	NGC4501	UGC07675	7.08	2598
18285	UGC09025		1.00	18285
18148	UGC10250		0.93	19446
18117	NGC3968	UGC06895	2.69	6731
18114	UGC01886		3.89	4656
18113	NGC6007	UGC10079	1.70	10666
18078	NGC3314B		3.80	4755
17738	UGC09107		1.15	15449
17481	NGC1365		11.22	1558
17156	Anon0958-14		1.82	9428
16912	NGC0309		3.16	5348
16847	PGC07941		2.63	6405
16804	UGC01810	Anon0218+39A	2.29	7335
16772	NGC7753	UGC12780	3.47	4837
16740	UGC03252		2.75	6078
16620	UGCA228	Anon1108-09	2.04	8140
16598	NGC0772	UGC01466	7.59	2188
16546	NGC5514	UGC09102	2.19	7563
16395	IC3165	UGC07384	1.91	8604
16279	NGC2336	UGC03809	7.41	2196
16273	NGC6744		20.42	797

TABLE 2—*Continued*

$a \times V$	Name	Alt. Name	$a$ arcmin	$V_{3K}$ $\text{km s}^{-1}$
16191	NGC4535	UGC07727	7.08	2287
16084	UGC02351		1.95	8249
16020	UGC08510		1.10	14610
15884	UGC04207		1.66	9571
15865	NGC6177	UGC10428	1.70	9342
15783	NGC5652	UGC09334	2.04	7730
15760	NGC6632	UGC11226	3.39	4651
15692	IC1222	UGC10461	1.70	9240
15599	NGC5230	UGC08573	2.19	7130
15445	NGC6674	UGC11308	4.68	3302

TABLE 3  
GALAXIES OBSERVED

Name	Alt. Name	PA deg.	err. deg.	Incl. deg.	err. deg.	Description	Type	Notes
Anon0958–14		...	...	...	...	2-arm g.d.	Bp	(1)
ESO437–G044	AM1039–283	...	...	0	...	2-arm g.d.	S	
IC0167	UGC01313	86	3	49	2	2-arm g.d.	B	(1,3)
IC0211	UGC01678	39	3	46	2	2-arm g.d.	Bp	
IC0267	UGC02368	14	7	37	3	2-arm g.d.	B	
IC0421	UGCA111	...	...	0	...	mixed	Bp	
IC0983	UGC09061	...	...	0	...	multiple arms	Bp	
IC1142	UGC10055	148	10	32	7	multiple arms	Bp	
IC1237	UGC10621	20	1	71	1	2-arm g.d.	B:p:	(4)
IC1302		43	3	59	2	2-arm g.d.	S	
IC1516	UGC12852	45	17	11	6	multiple arms	Sr	
IC1525	UGC12883	26	5	30	6	2-arm g.d.	Bp	
IC1551	UGC00268	...	...	...	...	two tidal arms	S	(2)
IC2421	UGC04658	61	31	22	12	2-arm g.d.	S	(3)
IC2627	UGCA227	134	15	34	4	2-arm g.d.	S	
IC4381	UGC09073	126	6	50	5	2-arm g.d.	S	(3)
NGC0036	UGC00106	9	1	61	2	2-arm g.d.	Bp	
NGC0132	UGC00301	46	3	39	2	2-arm g.d.	B:	
NGC0173	UGC00369	94	5	37	5	2-arm g.d.	S	
NGC0180	UGC00380	158	4	32	3	mixed	Bp	
NGC0266	UGC00508	118	8	17	5	2-arm g.d.	Bp:	
NGC0280	UGC00534	104	5	51	4	2-arm g.d.	S	
NGC0497	UGC00915	131	4	58	2	multiple arms	Bp	
NGC0521	UGC00962	...	...	0	...	mixed	Bp:	
NGC0536	UGC01013	63	2	70	2	2-arm g.d.	Br	
NGC0562	UGC01049	6	26	18	10	2-arm g.d.	S	
NGC0606	UGC01126	109	6	30	9	3-arm g.d.	Bp	
NGC0753	UGC01437	121	7	46	0	multiple arms	S	
NGC0772	UGC01466	120	4	47	1	not regular	S	
NGC0841	UGC01676	131	1	61	1	2-arm g.d.	P:Sr	
NGC1042		182	11	20	8	2-arm g.d.	S	
NGC1169	UGC02503	34	4	46	2	multiple arms	Br	
NGC1376		...	...	0	1	multiple arms	S	
NGC1417		6	2	62	1	2-arm g.d.	B:p	
NGC1784		111	6	35	5	multiple arms	Br	
NGC2206	UGCA123	134	3	54	2	2-arm g.d.	Sr	
NGC2280	UGCA131	158	4	65	2	2-arm g.d.	S	(1,4)
NGC2336	UGC03809	182	2	52	1	multiple arms	Sp	
NGC2460	UGC04097	17	3 <sub>22</sub>	45	3	mixed	S	
NGC2535	UGC04264	...	...	...	...	2-arm g.d.	Sp	(2)

TABLE 3—*Continued*

Name	Alt. Name	PA deg.	err. deg.	Incl. deg.	err. deg.	Description	Type	Notes
NGC2543	UGC04273	42	4	51	2	2-arm g.d.	B	
NGC2595	UGC04422	41	7	42	1	2-arm g.d.	Bp	
NGC2608	UGC04484	43	3	38	1	multiple arms	Bp:	
NGC2713	UGC04691	107	2	66	1	2-arm g.d.	Br	
NGC2718	UGC04707	88	21	19	16	2-arm g.d.	Br	
NGC2935	UGCA169	167	3	31	3	2-arm g.d.	B	
NGC3038		121	2	56	2	mixed	S	
NGC3054	UGCA187	120	3	49	2	2-arm g.d.	B	
NGC3183	UGC05582	155	7	40	10	2-arm g.d.	B	
NGC3319	UGC05789	39	2	55	2	2-arm g.d.	B	
NGC3347		175	3	64	3	2-arm g.d.	Bp	(3)
NGC3381	UGC05909	75	20	17	16	2-arm g.d.	B	
NGC3433	UGC05981	46	8	37	2	2-arm g.d.	S	
NGC3478	UGC06069	131	2	60	2	multiple arms	B	
NGC3513	UGCA224	92	5	36	6	2-arm g.d.	Bp	
NGC3577	UGC06257	...	...	2	2	2-arm g.d.	Bp	
NGC3583	UGC06263	124	4	38	1	2-arm g.d.	B	
NGC3642	UGC06385	35	35	5	5	2-arm g.d.	S	
NGC3883	UGC06754	160	12	34	4	mixed	B	
NGC3897	UGC06784	92	2	35	4	2-arm g.d.	Sp	
NGC3963	UGC06884	...	...	0	...	2-arm g.d.	B	
NGC3968	UGC06895	7	3	48	3	multiple arms	B	
NGC3992	UGC06937	69	1	53	1	multiple arms	Bp	
NGC4079	UGC07067	127	2	46	4	2-arm g.d.	S	
NGC4321	UGC07450	27	8	33	1	2-arm g.d.	B	
NGC4662	UGC07917	137	10	13	7	multiple arms	Bp	
NGC5172	UGC08477	95	1	50	1	one-armed	S	
NGC5230	UGC08573	...	...	2	2	multiple arms	Br	
NGC5248	UGC08616	99	3	36	2	2-arm g.d.	S	
NGC5409	UGC08938	41	3	46	5	2-arm g.d.	Sr	
NGC5619	UGC09255	6	1	62	3	2-arm g.d.	Bp	
NGC5829	UGC09673	55	6	32	5	2-arm g.d.	S	
NGC5905	UGC09797	128	5	34	3	2-arm g.d.	Bp	
NGC6177	UGC10428	23	3	43	3	2-arm g.d.	BPr	
NGC6181	UGC10439	2	1	61	2	2-arm g.d.	B	
NGC6412	UGC10897	49	28	7	7	2-arm g.d.	B	
NGC6632	UGC11226	150	2	59	1	two patterns?	Sp	
NGC6674	UGC11308	137	3	50	1	multiple arms	Br	
NGC6907	UGCA418	97	35	17	15	2-arm g.d.	B:	
NGC6951	UGC11604	150	6	31	3	2-arm g.d.	Bp	

TABLE 3—*Continued*

Name	Alt. Name	PA deg.	err. deg.	Incl. deg.	err. deg.	Description	Type	Notes
NGC6956	UGC11619	122	32	16	8	2-arm g.d.	Br	
NGC6962	UGC11628	77	1	38	2	2-arm g.d.	B	
NGC7042	UGC11702	128	3	35	2	2-arm g.d.	S	
NGC7309		138	66	12	12	3-arm g.d.	S	
NGC7407	UGC12230	151	1	61	2	2-arm g.d.	S	
NGC7685	UGC12638	176	14	40	5	2-arm g.d.	Sr	
NGC7738	UGC12757	70	7	52	2	2-arm g.d.	BP	
NGC7743	UGC12759	114	9	29	4	2-arm g.d.	BP	
NGC7753	UGC12780	33	3	47	3	2-arm g.d.	B	
NGC7769	UGC12808	25	7	25	11	mixed	S	
NGC7782	UGC12834	178	2	54	2	faint	S	
NGC7819	UGC00026	105	3	43	4	2-arm g.d.	B	
UGC00250		125	1	48	3	multiple arms	Br	
UGC00520		138	1	60	1	2-arm g.d.	S	
UGC00850		65	4	58	2	2-arm g.d.	B:r	(3)
UGC01919		35	10	33	4	2-arm g.d.	Br	
UGC02151		109	1	59	1	three arms	S	
UGC02507		5	2	55	1	2-arm g.d.	B	
UGC02582		10	9	22	14	multiple arms	S	
UGC02885		44	1	65	1	multiple arms	B:	
UGC03120		115	2	41	2	2- or 3-arm g.d.	S	
UGC03252		40	3	41	2	mixed	S	
UGC03294		125	2	61	5	multiple arms	Br	
UGC03325		34	6	32	0	2-arm g.d.	B:	
UGC03374		33	24	16	14	2-arm g.d.	Br	
UGC03375		49	1	61	1	multiple arms	B:p	
UGC03531		139	2	48	3	2-arm g.d.	Br	
UGC03593		46	1	58	2	2-arm g.d.	S	
UGC04207		21	6	56	2	2-arm g.d.	Sr	
UGC04219		122	3	42	4	2-arm g.d.	S	
UGC04457	Anon0829+19A	171	9	52	3	2-arm g.d.	S	
UGC04643		94	5	36	4	2-arm g.d.	S	
UGC04706		130	10	33	9	2-arm g.d.	B	
UGC04884		41	4	47	3	2-arm g.d.	S	
UGC05813		40	3	52	3	multiple arms	Br	
UGC06093		...	...	1	1	2-arm g.d.	Br	(1)
UGC07065		144	1	35	2	2-arm g.d.	BPr	(1,3)
UGC08058	Anon1254+57	...	...	...	...	2-arm g.d.	S	(2)
UGC08510		...	...	9	9	multiple arms	S	
UGC09025		64	3	53	3	multiple arms	B:	



TABLE 3—*Continued*

Name	Alt. Name	PA deg.	err. deg.	Incl. deg.	err. deg.	Description	Type	Notes
UGC09107		150	6	45	4	2-arm g.d.	Sr	(3)
UGC09808		...	...	0	...	2-arm g.d.	S	
UGC10104	Anon1555+30	19	36	9	9	2-arm g.d.	S	
UGC10405		40	9	37	3	multiple arms	B	
UGC10837		151	1	59	2	2-arm g.d.	Bp:	
UGC11406		7	3	53	4	2-arm g.d.	B	
UGC11453	Anon1930+54	79	1	40	1	2-arm g.d.	S	
UGC11473		128	4	62	2	not regular	S	
UGC11585		82	2	48	3	2-arm g.d.	Br	
UGC11695	Anon2109-01	107	4	56	4	2-arm g.d.	S	
UGC11809		31	1	61	0	not regular	B	
UGC11919	Anon2206+40	23	6	44	4	2-arm g.d.	S	
UGC12084		96	14	30	7	2-arm g.d.	Br	
UGC12128		130	1	61	0	2-arm g.d.	S	
UGC12164		121	3	52	2	2-arm g.d.	S	
UGC12199		95	4	55	1	2-arm g.d.	Br	
UGC12646		48	1	23	7	2-arm g.d.	BPr	
UGC12776		95	12	37	4	2-arm g.d.	Br	
UGC12792		56	10	42	2	2-arm g.d.	BR	
UGCA228	Anon1108-09	10	51	8	8	multiple arms	Bp	

NOTE.—“g.d.” means “grand design”; “mixed” means having both 2-armed grand design and multiple arm morphology in different parts of the disk; (1) exposure is insufficient to show reliable outer isophotes; (2) merger, interacting, or tidal, not deprojected; (3) spiral structure influences shape of outer isophotes; (4) deprojected according to inner disk isophotes.

TABLE 4  
SPIRAL EXTENT

Name	Alt. Name	$R_1$ arcsec	$R_2$ arcsec	Eq. 7	Pass?	Eq. 12	Pass?	S/N	Notes
Anon0958-14		7	51	2.06	N	1.21	.	3.0	(1)
ESO437-G044	AM1039-283	25	112	1.31	.	0.77	.	1.6	(1)
IC0167	UGC01313	13	104	2.41	N	1.36	.	6.8	(10)
IC0211	UGC01678	7	65	2.78	N	1.57	.	14.0	
IC0267	UGC02368	56	83	0.43	.	0.24	.	5.8	
IC0421	UGCA111	21	73	1.02	.	0.57	.	9.3	(7,8)
IC1237	UGC10621	13	69	1.55	.	0.87	.	10.9	(4)
IC1302		9	28	0.94	.	0.53	.	11.6	
IC1525	UGC12883	14	51	1.05	.	0.59	.	14.0	
IC1551	UGC00268	16	77	1.39	.	0.81	.	3.0	(1,10)
IC2421	UGC04658	22	63	0.84	.	0.49	.	3.0	(10)
IC2627	UGCA227	14	85	1.79	~	1.05	.	5.5	(4)
		14	105	2.21	N	1.30	.	3.0	(3,12)
IC4381	UGC09073	12	61	1.47	.	0.86	.	2.4	(4,5)
NGC0036	UGC00369	18	85	1.37	.	0.80	.	4.0	(2)
NGC0132	UGC00301	8	56	2.19	N	1.28	.	2.8	(14)
NGC0173	UGC00369	15	110	2.18	N	1.23	.	3.1	
NGC0180	UGC00380	15	30	0.59	.	0.33	.	39.7	(7,8)
NGC0266	UGC00508	34	108	0.94	.	0.55	.	5.3	
NGC0280	UGC00534	11	42	1.09	.	0.64	.	23.9	
NGC0521	UGC00962	19	44	0.68	.	0.40	.	14.9	(2,7,8)
NGC0536	UGC01013	63	100	0.47	.	0.27	.	11.1	
NGC0562	UGC01049	6	33	1.68	.	0.95	.	16.9	(4)
NGC0841	UGC01676	25	45	0.52	.	0.30	.	5.5	
NGC1042		12	94	2.38	N	1.39	.	8.1	
NGC1417		15	73	1.46	.	0.85	.	8.3	
NGC2206	UGCA123	20	67	0.99	.	0.58	.	12.3	
NGC2280	UGCA131	22	72	0.99	.	0.58	.	66.9	(2,8)
		22	243	3.31	N	1.94	~	4.4	(3,7)
NGC2460	UGC04097	82	160	0.57	.	0.34	.	4.7	(5,9)
NGC2535	UGC04264	20	160	2.41	N	1.41	.	4.2	(1)
NGC2543	UGC04273	23	90	1.15	.	0.65	.	3.5	(3)
NGC2595	UGC04422	33	88	0.77	.	0.45	.	4.8	
NGC2713	UGC04691	45	74	0.49	.	0.28	.	24.7	
NGC2718	UGC04707	32	48	0.44	.	0.26	.	11.6	
NGC2935	UGCA169	43	130	0.89	.	0.50	.	8.9	(2)
		43	155	1.06	.	0.60	.	1.2	(3)
NGC3038		34	78	0.67	.	0.38	.	14.0	(9,16)
NGC3054	UGCA187	19	63 <sub>26</sub>	0.99	.	0.58	.	23.5	(7,8)
		19	98	1.54	.	0.90	.	8.3	(3,12)

TABLE 4—*Continued*

Name	Alt. Name	$R_1$ arcsec	$R_2$ arcsec	Eq. 7	Pass?	Eq. 12	Pass?	S/N	Notes
NGC3183	UGC05582	27	61	0.67	.	0.39	.	18.6	
NGC3319	UGC05789	56	170	0.89	.	0.52	.	12.8	
NGC3347		74	131	0.52	.	0.30	.	67.5	
NGC3381	UGC05909	14	43	0.90	.	0.53	.	15.3	
NGC3433	UGC05981	21	49	0.68	.	0.40	.	31.8	(7,8)
NGC3513	UGCA224	22	93	1.25	.	0.70	.	13.3	
NGC3577	UGC06257	12	52	1.29	.	0.72	.	1.2	
NGC3583	UGC06263	27	68	0.75	.	0.42	.	32.6	
NGC3642	UGC06385	28	128	1.35	.	0.76	.	11.3	(3)
NGC3883	UGC06754	18	40	0.63	.	0.37	.	8.2	(7,8)
NGC3897	UGC06784	12	71	1.82	~	1.06	.	3.1	
NGC3963	UGC06884	18	66	1.08	.	0.61	.	12.8	
NGC4079	UGC07067	12	75	1.76	~	1.03	.	5.0	
NGC4321	UGC07450	60	155	0.76	.	0.44	.	39.7	
NGC5248	UGC08616	28	100	1.06	.	0.62	.	103.9	(8)
		100	219	0.64	.	0.38	.	3.8	(5)
NGC5409	UGC08938	21	41	0.58	.	0.34	.	10.1	
NGC5619	UGC09255	27	59	0.64	.	0.38	.	21.2	
NGC5829	UGC09673	5	52	3.10	N	1.75	~	14.4	
NGC5905	UGC09797	27	105	1.14	.	0.67	.	5.4	(2)
		27	128	1.40	.	0.82	.	4.7	(3,12)
NGC6177	UGC10428	23	44	0.56	.	0.33	.	14.1	
NGC6181	UGC10439	22	59	0.79	.	0.44	.	10.4	(4)
NGC6412	UGC10897	10	53	1.52	.	0.85	.	27.2	
NGC6632	UGC11226	27	42	0.46	.	0.27	.	33.1	(8)
		55	88	0.47	.	0.27	.	16.4	(5)
NGC6907	UGCA418	11	107	2.85	N	1.67	.	5.1	
NGC6951	UGC11604	54	107	0.59	.	0.34	.	3.7	
NGC6956	UGC11619	20	46	0.68	.	0.40	.	15.1	
NGC6962	UGC11628	42	73	0.51	.	0.30	.	15.1	
NGC7042	UGC11702	10	49	1.40	.	0.82	.	25.1	
NGC7407	UGC12230	10	30	0.88	.	0.52	.	21.2	(2)
NGC7685	UGC12638	10	67	2.05	N	1.16	.	5.2	(4)
NGC7738	UGC12757	42	65	0.46	.	0.27	.	3.3	
NGC7743	UGC12759	39	55	0.42	.	0.24	.	20.9	
NGC7753	UGC12780	23	101	1.31	.	0.77	.	8.0	
NGC7769	UGC12808	28	94	1.00	.	0.58	.	4.2	(9,10,16)
NGC7819	UGC00026	21	52	0.74	.	0.43	.	7.6	
UGC00520		10	17	0.50	.	0.29	.	7.3	
UGC00850		7	31	1.30	.	0.76	.	12.9	

TABLE 4—*Continued*

Name	Alt. Name	$R_1$ arcsec	$R_2$ arcsec	Eq. 7	Pass?	Eq. 12	Pass?	S/N	Notes
UGC01919		19	35	0.54	.	0.32	.	5.9	
UGC02507		14	27	0.56	.	0.33	.	9.0	(2)
		14	32	0.66	.	0.39	.	4.3	(3,11)
UGC03252		13	27	0.63	.	0.37	.	68.7	(7,8)
UGC03325		9	38	1.19	.	0.70	.	4.9	
UGC03374		41	71	0.50	.	0.28	.	4.0	(4)
UGC03531		15	45	0.88	.	0.52	.	5.5	
UGC03593		11	34	0.91	.	0.51	.	25.5	
UGC04207		13	48	1.05	.	0.59	.	5.3	(2)
UGC04219		13	64	1.49	.	0.87	.	1.6	
UGC04457		7	66	2.80	N	1.64	.	3.5	(10)
UGC04643		10	63	1.89	~	1.07	.	5.2	
UGC04706		23	40	0.52	.	0.30	.	4.6	
UGC04884		23	30	0.38	.	0.21	.	8.2	
UGC06093		8	36	1.32	.	0.77	.	2.7	
UGC07065		26	54	0.61	.	0.34	.	6.6	
UGC09107		17	42	0.74	.	0.43	.	4.8	
UGC09808		7	45	1.87	~	1.05	.	6.2	(4)
UGC10104	Anon1555+30	10	75	2.20	N	1.24	.	5.0	
UGC10837		25	54	0.65	.	0.38	.	5.1	
UGC11406	Anon1906+42	46	71	0.45	.	0.25	.	19.7	
UGC11453	Anon1930+54	23	57	0.73	.	0.41	.	19.4	(10)
UGC11585		15	34	0.66	.	0.39	.	15.2	
UGC11695	Anon2109-01	10	28	0.84	.	0.49	.	5.8	(4,13)
		10	56	1.70	.	1.00	.	2.4	(10,14)
UGC11919	Anon2206+40	10	37	1.04	.	0.61	.	13.8	
UGC12084		19	35	0.54	.	0.32	.	4.4	
UGC12128		20	28	0.42	.	0.24	.	3.1	
UGC12164		17	58	1.02	.	0.60	.	6.1	
UGC12199		35	49	0.42	.	0.23	.	11.2	
UGC12646		31	44	0.42	.	0.25	.	6.3	
UGC12776		47	121	0.76	.	0.43	.	3.3	
UGC12792		11	22	0.61	.	0.35	.	11.7	

NOTE.—In the “Pass?” columns, “.” means the ratio passes the “conservative” ratio test (§2.2), “~” means the ratio is marginally in violation (value between 1.71 and 2), and “N” means the ratio fails the conservative test. (1) not deprojected; (2) main pattern or bright arms only; (3) including faint or broad arms in outer disk; (4) some irregularity, regular arms only; (5) two patterns, outer pattern only; (6) includes both 2-arm patterns; (7) outer disk has multiple arms; (8) inner 2-arm pattern only; (9) inner disk has multiple arms; (10) possibly tidal or interacting; (11) extension of main 2-arm pattern; (12) detached from main 2-arm pattern; (13) shorter of two arms; (14) longer of two arms; (15) deprojection may not be appropriate; (16) outer two-arm pattern.

TABLE 5  
 SPIRAL ARM BRIGHTNESS AT OUTER EXTENT

Name	Alt. Name	$\mu_V$ mag arcsec <sup>-2</sup>
IC0167	UGC01313	26.0
IC0267	UGC02368	26.5
NGC0266	UGC00508	25.6
NGC0521	UGC00962	22.5
NGC2543	UGC04273	25.2
NGC2595	UGC04422	25.1
NGC3883	UGC06754	23.6
NGC5905	UGC09797	25.7
NGC6181	UGC10439	23.3
NGC6951	UGC11604	23.8
NGC6962	UGC11628	23.2
NGC7685	UGC12638	25.9
NGC7743	UGC12759	22.6
NGC7769	UGC12808	25.5